

Accommodation of excess Ti in a (Ba,Sr)TiO₃ thin film with 53.4% Ti grown on Pt/SiO₂/Si by metalorganic chemical-vapor deposition

I. Levin^{a)}

Ceramics Division, National Institute of Standards and Technology, Gaithersburg, Maryland 20899

R. D. Leapman

Bioengineering and Physical Science Program, ORS, National Institutes of Health, Bethesda, Maryland 20892

D. L. Kaiser

Ceramics Division, National Institute of Standards and Technology, Gaithersburg, Maryland 20899

P. C. van Buskirk, S. Bilodeau, and R. Carl

Advanced Technology Materials, Inc., 7 Commerce Drive, Danbury, Connecticut 06810

(Received 13 January 1999; accepted for publication 7 July 1999)

The microstructure and chemistry of a Ti-rich (Ba,Sr)TiO₃ film with 53.4% Ti deposited on a Pt/SiO₂/Si substrate by metalorganic chemical-vapor deposition was studied using high-resolution transmission electron microscopy and elemental mapping in electron energy-loss spectroscopy. We established that the Ti/Ba ratio at *all* the grain boundaries in this film is significantly higher than that in the grain interiors. Structural images revealed the presence of disordered amorphous-like regions at some of the grain boundaries and triple junctions; these regions were tentatively identified as those having the highest Ti/Ba ratio in the chemical maps. Analysis of the electron energy-loss near-edge structure for the O-K edge indicated an increased titanium-to-oxygen coordination at the grain boundaries. No second phase was detected at the (Ba,Sr)TiO₃/Pt interface. © 1999 American Institute of Physics. [S0003-6951(99)01735-0]

Recently, much attention has been focused on the fabrication of polycrystalline thin films of barium strontium titanate Ba_{1-x}Sr_xTiO₃.¹⁻⁷ This material can offer a high dielectric permittivity at a relatively large thickness in dynamic random access memories,⁶⁻⁸ and has properties of interest for tunable microwave devices.⁷ Deviation of the (Ba+Sr)/Ti ratio from the stoichiometric value of unity is reported to have a dramatic effect on the dielectric properties.⁹ For example, the dielectric constant of 40-nm-thick films decreases by about 60% when the Ti content is increased from 51 to 53.5 at. %. This effect is even more pronounced for larger film thicknesses. Despite this dramatic effect of stoichiometry on the dielectric properties, the mechanism for accommodating excess Ti in these films has not been determined. In this letter we report preliminary results of an on-going study in which both high-resolution transmission electron microscopy and elemental mapping in electron energy-loss spectroscopy are applied to address this issue.

The (Ba,Sr)TiO₃ (BST) thin film was deposited on a Pt(100 nm)/SiO₂/Si substrate by liquid-delivery metalorganic chemical-vapor deposition (MOCVD) at a substrate temperature of 640 °C.² Wavelength-dispersive x-ray fluorescence spectroscopy measurements gave elemental concentrations of Ba, Sr, and Ti in the film of 33.20±0.44, 13.35±0.1, and 53.45±0.22 at. %, respectively, and a BST film thickness of 38.7 nm.

Both planar-view and cross-sectional transmission electron microscopy specimens were prepared by conventional grinding and polishing, followed by dimpling to a thickness of 30 μm. The specimens were further thinned to perforation

in a Gatan¹⁰ precision ion-polishing system (PIPS) at a voltage of 5 kV and an angle of 4.5°. Planar-view specimens were ion thinned from the substrate side only, with the other side protected by a thin single-crystal MgO wafer to prevent contamination.

Structural imaging was performed in a JEOL 3010UHR (300 kV) high-resolution transmission electron microscope. A VG-HB501 dedicated scanning transmission electron microscope (STEM) equipped with a cold field-emission gun and a Gatan parallel-detection electron energy-loss spectrometer was used for chemical analysis.¹¹ The specimen was cooled to liquid-nitrogen temperature to prevent contamination. Spectrum images (64×64 pixels) were recorded by scanning a focused electron probe of approximately 1.5 nm diam over an area of about 80 nm×80 nm. Spectra in the energy-loss range from 400 to 800 eV (which includes Ti L_{2,3}, O-K, and Ba-M_{4,5} edges), were acquired at each point (pixel). Specimen drift during the data acquisition was corrected by using a cross-correlation procedure implemented in the Gatan software.¹² The spectrum images were subsequently processed to remove the background, and maps of both the Ti-L_{2,3} and Ba M_{4,5} intensity distributions were obtained by integrating the corresponding edges over an energy window of 50 eV.

Electron diffraction from the planar-view and cross-sectional specimens showed that both the Pt and BST films were highly textured with the <001>_{BST} and <111>_{Pt} directions preferentially aligned parallel to the surface normal. No preferred in-plane orientation relationship between the Pt and BST grains was detected.

Examination of the cross-sectional specimens showed that the BST film was composed of columnar grains [Fig.

^{a)}Electronic mail: igorl@mailserver.nist.gov

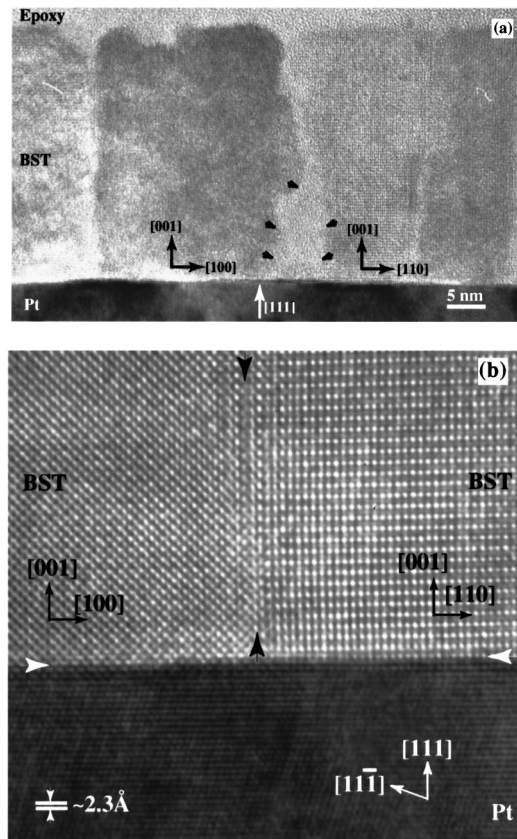


FIG. 1. (a) Intermediate magnification phase contrast image of the Ti-rich BST film on a Pt/SiO₂/Si substrate (cross-sectional specimen). A region with amorphous-like contrast is indicated by arrows. (b) High-magnification phase contrast image of the BST/Pt interface. Black and white arrows indicate the boundary between two adjacent BST grains and the BST/Pt interface, correspondingly.

1(a)] with widths in the range of 10–20 nm, that extended through the entire film thickness of ≈ 39 nm (measured from the image). No second phase or amorphous interlayer was observed at the BST/Pt interface [Fig. 1(b)], but some of the BST grain boundaries in the cross-sectional specimen contained small “pockets,” 2–3 nm in size, with amorphous-like contrast [arrows, Fig. 1(a)].

A typical phase contrast image of the planar-view specimen recorded at low magnification is shown in Fig. 2(a). All of the grains in this image are close to the [001] zone-axis orientation and the grain boundaries are nearly parallel to the beam direction. Most of the grain boundaries show a prominent bright contrast as compared to the interior of the grains. Structural images recorded at higher magnification [Fig. 2(b)] revealed the presence of a disordered layer (~ 1 nm) at many of these tilt boundaries, while pockets (1–3 nm) with amorphous-like contrast often were identified at the triple junctions, consistent with the observations made on the cross-sectional specimens. No other second phase was detected in either the cross-sectional or planar-view specimens. Structural imaging suggested the presence of three microstructural components in the film having distinct phase contrast: (1) the interior of the grains; (2) well-structured grain boundaries with no visible amorphous phase; and (3) regions at some grain boundaries and triple junctions with amorphous-like contrast [Fig. 2(b)].

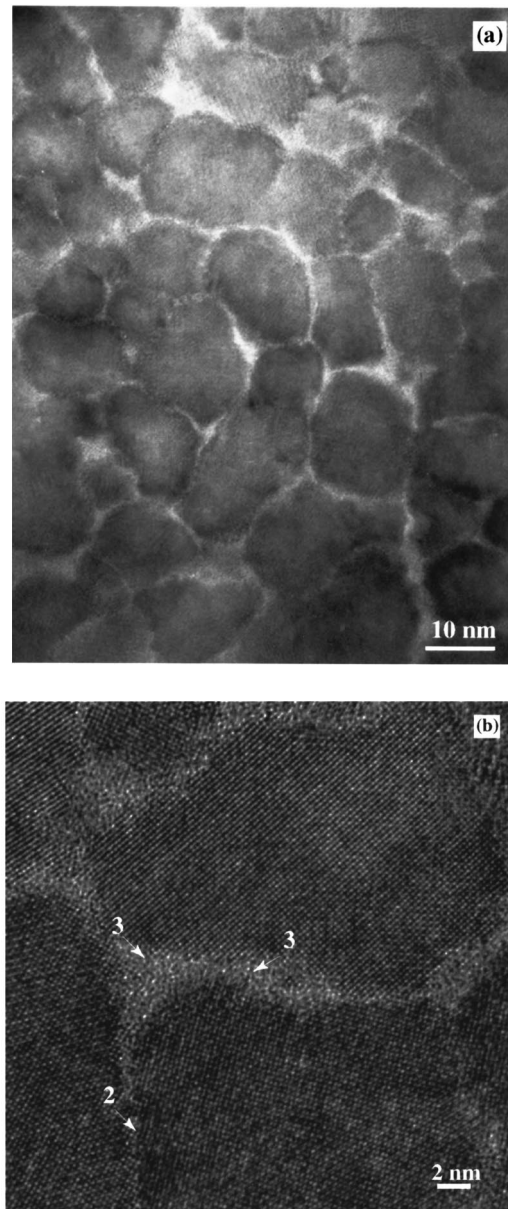


FIG. 2. (a) Low-magnification phase contrast image of the BST film (planar-view specimen). All grains are close to the [001] orientation. (b) High-magnification structural image of the same area. Disordered regions with amorphous-like contrast are observed at some of the grain boundaries and triple junctions (labeled “3”). Other grain boundaries are well structured (labeled “2”).

Figure 3 shows representative maps of both the Ti- $L_{2,3}$ (a) and Ba- $M_{4,5}$ (b) intensity distributions obtained from the planar-view specimen, and the calculated map of the Ti/Ba ratio (c). The elemental intensities maps suggest that all boundaries are Ba deficient [Fig. 3(b)], while only some of the boundaries have a higher Ti signal as compared to the grain interiors; note that the elemental signals are affected by both diffraction contrast and thickness variations across the analyzed area. The Ti/Ba ratio map [Fig. 3(c)], wherein all possible artifacts have been largely eliminated, clearly demonstrates that *all* of the grain boundaries have a significantly higher Ti/Ba ratio than that in the grain interiors. Analysis of this map suggests the presence of three regions with statistically different average Ti/Ba ratios: (a) the grain interiors (dark areas); (b) the grain boundaries and regions adjacent to

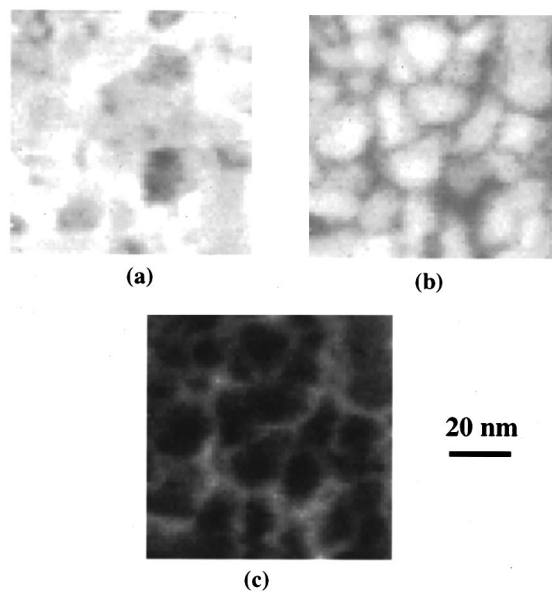


FIG. 3. Maps of Ti- $L_{2,3}$ (a) and Ba- $M_{4,5}$ (b) intensity distributions obtained using parallel electron energy-loss spectroscopy in STEM. (c) Calculated map of the Ti/Ba ratio.

them (dark-gray areas), which have a moderately higher Ti/Ba ratio than that of the grain interiors; and (c) regions at grain boundaries and triple junctions with the highest Ti/Ba ratio (light-gray areas).

The results of the chemical mapping measurements are consistent with the observations made using structural imaging, assuming that the dark, dark-gray, and light-gray regions in the Ti/Ba ratio map correspond to the microstructural components 1, 2, and 3, respectively. Bright contrast at the grain boundaries as observed in the structural images can be at least partially attributed to a lower mean-atomic density due to an increase in the Ti/Ba ratio. These results suggest that excess Ti in this film is accommodated through an increase in the concentration of Ba vacancies near and at the grain boundaries, consistent with reported observations on bulk material,¹³ and through the formation of Ti-rich amorphous-like regions at some of the grain boundaries and triple junctions. Increase in a concentration of Ba vacancies near the grain boundaries results in a negative space-charge region, which requires a positively charged grain boundary.¹³ It is not clear from the present data whether this positive charge at the grain boundary core is produced by an excess of Ti ions or a combination of both oxygen and barium vacancies with $[V_{\text{O}}^{\bullet}] > [V_{\text{Ba}}^{\prime\prime}]$ at the boundary, as proposed in Ref. 13.

Comparison of the electron energy-loss near-edge structure (ELNES) for the O- K edge recorded at the grain boundaries and in the grain interior (Fig. 4) revealed that the intensity of peak B, associated with a σ^* -type antibonding interaction between the oxygen and Ti atoms,¹⁴ is significantly higher in the spectrum from the boundary. The O- K ELNES recorded from the grain interiors [Fig. 4(a)] is similar to that reported for the bulk BaTiO₃ and SrTiO₃, both

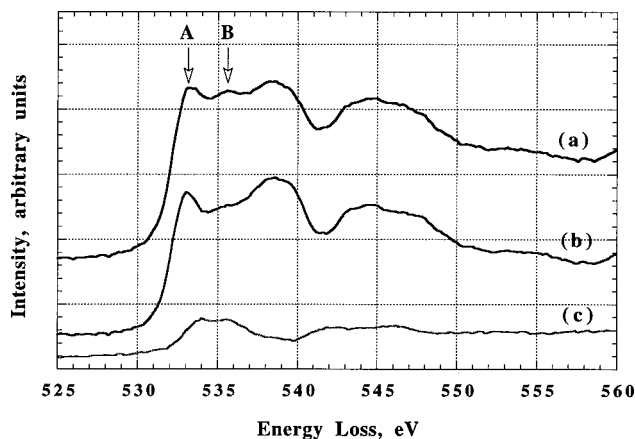


FIG. 4. O- K ELNES (a) at a grain boundary, (b) in the grain interior, and (c) a spatial difference between (a) and (b). Peaks "A" and "B" correspond to π^* and σ^* pd -type antibonding interactions between O and Ti.

having linear twofold coordination of titanium to oxygen.¹⁴ On the other hand, the O- K ELNES recorded from the boundaries [Figs. 4(a) and 4(c)] resembles that of TiO₂ polymorphs (rutile, brookite, and anatase) with the threefold coordination of titanium to oxygen.¹⁴ This result suggests that the coordination number of titanium to oxygen is higher at the boundaries compared to the grain interiors, which may be related to a change in the connectivity of TiO₆ octahedra at the boundary.

Studies are in progress to quantify the Ti/Ba ratio in different microstructural components in the film, to compare O- K ELNES for grain boundaries with different composition and to analyze the Ti/Ba distribution in BST films with Ti concentration closer to the stoichiometric value of 50%.

The discussions with G. Stauf (Advanced Technology Materials, Inc.), S. Streiffer (Argonne National Laboratory), and S. Stemmer (University of Illinois at Chicago) are acknowledged.

¹T. Kawahara, M. Yamamuka, T. Makita, J. Naka, A. Yuuki, N. Mikami, and K. Ono, *Jpn. J. Appl. Phys., Part 1* **33**, 5129 (1994).

²P. C. Van Buskirk, J. F. Roeder, and S. Bilodeau, *Integr. Ferroelectr.* **10**, 9 (1995).

³M. Yoshida, H. Yamaguchi, T. Sakuma, and Y. Miyasaka, *J. Electrochem. Soc.* **142**, 244 (1995).

⁴T. Horikawa, N. Mikami, T. Makita, J. Tanimura, M. Kataoka, K. Sato, and M. Nunoshita, *Jpn. J. Appl. Phys., Part 1* **32**, 4126 (1993).

⁵S. Yamamichi, J. Yabuta, T. Sakuma, and Y. Miyasaka, *Appl. Phys. Lett.* **64**, 1644 (1994).

⁶C. S. Hwang, S. O. Park, H.-J. Cho, C. S. Kang, S. I. Lee, and M. Y. Lee, *Appl. Phys. Lett.* **67**, 2819 (1995).

⁷J. S. Horwitz, W. Chang, A. C. Carter, J. M. Pond, S. W. Kirchoefer, D. B. Chrisey, J. Levy, and C. Hubert, *Integr. Ferroelectr.* **22**, 799 (1998).

⁸A. I. Kingon, S. K. Streiffer, C. Basceri, and S. R. Summerfelt, *Mater. Res. Bull.* **21**, 46 (1996).

⁹C. Basceri, Ph.D. thesis, North Carolina State University (1997), p. 171.

¹⁰The use of brand or trade names does not imply endorsement of the product by NIST.

¹¹R. D. Leapman and D. E. Newbury, *Anal. Chem.* **65**, 2409 (1993).

¹²J. A. Hunt and R. Harmon, *Ultramicroscopy* (in press).

¹³Y.-M. Chiang and T. Takagi, *J. Am. Ceram. Soc.* **73**, 3278 (1990).

¹⁴R. Brydson, H. Sauer, W. Engel, and F. Hofer, *J. Phys.: Condens. Matter* **4**, 3429 (1992).